Crack engineering for the construction of arbitrary hierarchical architectures

Wanbo Li[a,b,1], Miao Yu[c,1], Jing Sun[b,1], Kentaro Mochizuki[d], Siyu Chen[a], Huanxi Zheng[b], Jiaqian Li[b], Shuhuai Yao[c], Hongkai Wu[e], Beng S. Ong[a], Satoshi Kawata[d], Zuankai Wang[b,2], and Kangning Ren[a,f,g,2]

[a]Department of Chemistry, Hong Kong Baptist University, Kowloon, 999077 Hong Kong, China; [b]Department of Mechanical Engineering, City University of Hong Kong, Kowloon, 999077 Hong Kong, China; [c]Department of Mechanical and Aerospace Engineering, The Hong Kong University of Science and Technology, Kowloon, 999077 Hong Kong, China; [d]Department of Applied Physics, Osaka University, Suita, Osaka 565-0871, Japan; [e]Department of Chemistry, Hong Kong University of Science and Technology, Kowloon, 999077 Hong Kong, China; [f]State Key Laboratory of Environmental and Biological Analysis, Hong Kong Baptist University, Kowloon, 999077 Hong Kong, China; and [g]HKBU Institute of Research and Continuing Education, Hong Kong Baptist University, 518057 Shenzhen, China

Edited by David A. Weitz, Harvard University, Cambridge, MA, and approved October 14, 2019 (received for review September 6, 2019)

Three-dimensional hierarchical morphologies widely exist in natural and biomimetic materials, which impart preferential functions including liquid and mass transport, energy conversion, and signal transmission for various applications. While notable progress has been made in the design and manufacturing of various hierarchical materials, the state-of-the-art approaches suffer from limited materials selection, high costs, as well as low processing throughput. Herein, by harnessing the configurable elastic crack engineering—controlled formation and configuration of cracks in elastic materials—an effect normally avoided in various industrial processes, we report the development of a facile and powerful technique that enables the faithful transfer of arbitrary hierarchical structures with broad material compatibility and structural and functional integrity. Our work paves the way for the cost-effective, large-scale production of a variety of flexible, inexpensive, and transparent 3D hierarchical and biomimetic materials.

configurable elastic crack engineering | true 3D replication | hierarchical structures | biomimetic materials

Three-dimensional hierarchical structures are the fundamental elements of numerous biological and artificial surfaces that exhibit various fascinating functionalities useful for liquid and mass transport (1–7), adhesion (8–11), signal transformation (12), structural coloration (13, 14), etc. For instance, many living organisms evolved exquisite structures and functional materials for surviving in harsh environments (15). One extreme case is the evolution of reentrant structures that show superior repellence to liquids even with ultralow surface tension. The manifestation of these special architecture enables the skin of springtail beetles to repel various liquids and dirt, and respire in humid and dirty environment (1, 5). Another extreme case is exemplified by *Nepenthes alata* that evolved peristome arrays to offer the spontaneous, diode-like spreading of liquid (6, 7). The diversity and complexity of structures result in many unexpected combinations of functions, allowing biological systems to survive and adapt to the challenges of life.

In recent years, extensive efforts have been directed toward reproduction of these representative architectures, which is of importance to the creation of a wide spectrum of biomimetic and smart materials for practical applications (2–4, 9, 16, 17). While breakthroughs in bioinspired engineering have achieved a wide range of structures that enable various fascinating functionalities, it remains a daunting challenge to mimic structural hierarchy, material diversity, and functional sophistication of living organisms in a facile and reproducible manner. So far, these exquisite morphologies are generally achieved on rigid materials such as polystyrene (PS) (2) and silicon (3, 16, 17) using expensive and sophisticated microfabrication technologies and/or 2-photon 3D printing technologies. More importantly, these rigid engineered structures are mechanically vulnerable to external load because of the concentration of high local stress during their deformation, chemically susceptible to corrosives, topologically limited, and optically less attractive, thereby preventing real-life applications. Thus, it is timely to develop affordable and scalable strategies that enable the attainment of structural and functional diversity on more diversified materials.

In one of the most commonly used fabrication strategies, replication, the formation of cracks has normally been avoided due to its detrimental nature. However, 3D hierarchical structures commonly consist of a variety of deadlocking regions (e.g., closed loop, reentrant, high-aspect-ratio rods, and arrays), which can easily trigger the uncontrolled crack formation and subsequent structural failure during replication. Previous studies have also shown that proper control of crack formation in rigid materials can give rise to useful functionalities (18–22) such as atomic-scale pattern formation. Inspired by these studies, we develop a technique, termed as configurable, elastic crack engineering (CECE), which transforms the detrimental crack effect into a powerful tool for the faithful, scalable, and cost-effective fabrication of various hierarchical structures on a wide range of materials. As an immediate implementation, we also develop superrepellant surfaces and liquid diode devices with unprecedented functionalities.

Significance

Despite emerging breakthroughs in the achievement of numerous elegant biomimetic structures that impart fascinating functionalities, bioinspired materials still suffer from poor structural durability, chemical reliability, flexibility, and optical transparency, as well as unaffordable cost and low throughput, thus preventing their broad real-life applications. In striking contrast to conventional wisdom, we demonstrate that the usually avoided and detrimental elastic crack phenomenon can be translated into powerful configurable-crack engineering to achieve structures and functions that are impossible to realize even using state-of-the-art techniques. Our approach dramatically enriches the freedom and flexibility in the design of materials to mimic various natural living organisms and paves the road for translating nature's inspirations into real-world applications.

Author contributions: W.L., W.Z., and K.R. designed research; W.L., M.Y., J.S., K.M., S.C., H.Z., and J.L. performed research; W.L., M.Y., S.C., S.Y., H.W., B.S.O., and S.K. analyzed data; and W.L., Z.W., and K.R. wrote the paper.

The authors declare no competing interest.

This article is a PNAS Direct Submission.

[1]W.L., M.Y., and J.S. contributed equally to this work.

[2]To whom correspondence may be addressed. Email: zuanwang@cityu.edu.hk or kangningren@hkbu.edu.hk.

This article contains supporting information online at www.pnas.org/lookup/suppl/doi:10.1073/pnas.1915332116/-/DCSupplemental.

First published November 7, 2019.

Results

Concept of CECE. Our work mainly resorts to the unique features of elastomer materials, i.e., superior elastic deformation and a high level of configurability. Elastomers are usually amorphous, and thus tend to randomly crack when subject to stress during the replication process. To suppress the random cracks, we develop a modified soft lithography process (Fig. 1*A*) that enables the formation of a configurable intermediate state during the casting process, which allows a replica with true-3D shape to be produced using a master structure through a casting step followed by a molding step. The elastomer material in such an intermediate state fulfills 2 requirements simultaneously. On one hand, it is soft enough to bear a large elastic deformation and can spontaneously develop cracks at the preferential location to allow easy peeling from any master structure. On the other hand, it is rigid enough to regain its original shape for the reliable creation of final replicate structures.

Fig. 1 schematically illustrates the principle of CECE, in which a closed-loop structure is used as a master. Distinct from existing methods, CECE is a 2-phase process (Fig. 1*A* and *SI Appendix*, Fig. S1) characterized by 2 curing stages of the elastomer (Fig. 1*B* and *SI Appendix*, Fig. S2). The images in the upper row of Fig. 1*A* present the spontaneous formation of a crack in the elastomer in phase I when the closed loop is peeled off during the preparation of the polydimethylsiloxane (PDMS) mold of the master structure. The elastomer is cured at low temperature to give rise to a relatively lower density of cross-linking and looser macromolecular packing (23, 24). The Young's modulus of as-prepared elastomer is typically several orders of magnitude lower than that of the closed-loop master microstructure, which ensures that cracks are developed in the elastomer rather than in the master. During the peeling-off process, cracks are generated along the direction of the vertical peeling force. Since the subsequent molding process involves relatively high pressure, the elastomer mold needs to be self-sealable. Thus, to translate the intermediate elastomer into a

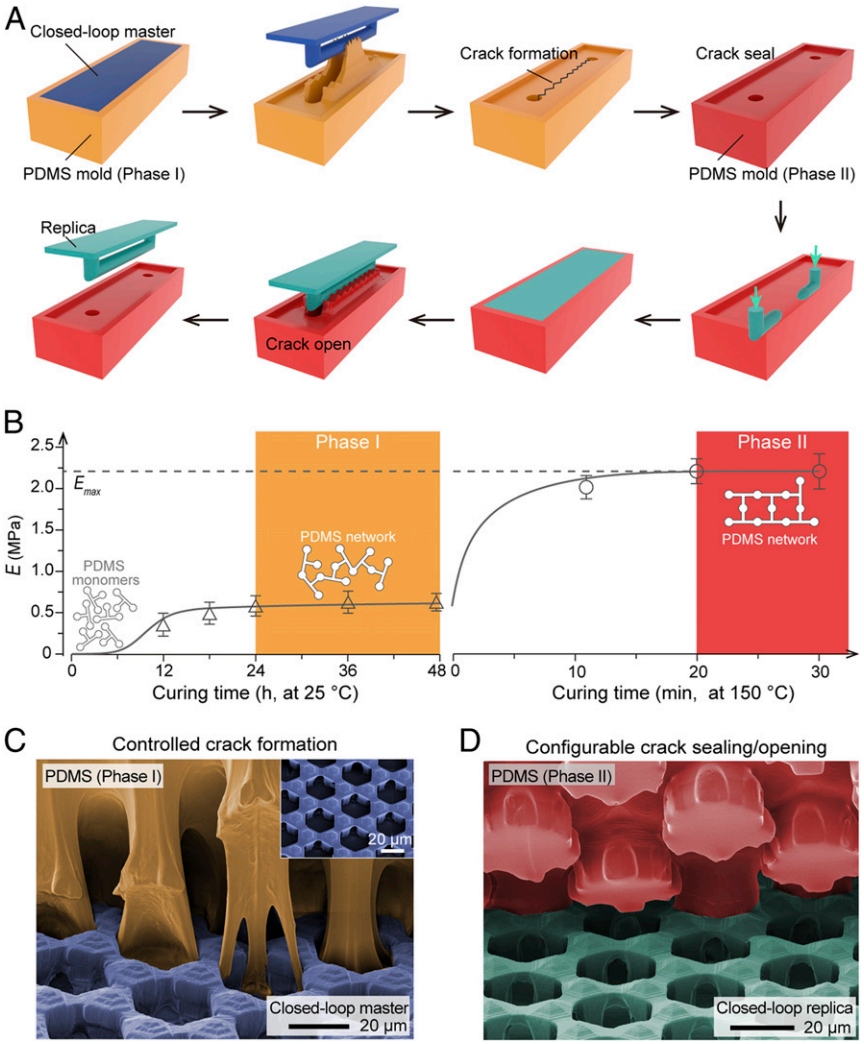

Fig. 1. CECE. (*A*) Schematic illustration of CECE for molding closed-loop structures. The upper row shows the controlled formation of the elastic crack in PDMS in a casting process to create a PDMS mold from the master (phase I). The lower row shows the configurable seal/open of the crack in PDMS in a molding process to create a replica of the master (phase II). In phase I, PDMS is prone to large elastic deformation and cracking; in phase II, PDMS is relatively rigid and can keep the conformality. (*B*) Molecular-level mechanism of dynamical manipulation of the mechanics of PDMS (phases I and II) by adjusting the curing temperature and curing time. The dashed line denotes maximum *E* of PDMS when fully cured at high temperature. Note that temperature plays the dominating role, leaving wide time windows for operation. (*C*) SEM images of the elastic crack formation in PDMS (phase I) being pulled out from an array of closed loops with diverse directions (*Inset*). (*D*) SEM image showing the process of separating PDMS (phase II) from the closed-loop replica. The elastic crack self-sealed during molding and multiple intact closed-loop replicas were obtained.

mature mold for the creation of 3D structure, we designed an additional curing step at higher temperature, denoted as phase II, to enhance the stiffness, self-sealing, and configurability of the elastomer. In this way, the crack keeps self-sealing during molding and regains its original shape after this entire process, and the shape and size of the as-formed elastic crack can be dynamically manipulated in phase II, where a molding process is used to create a replica of the master. On the other hand, phase I is proven necessary, as without it cracks are randomly formed without the preferred configurability, which is similar to the case of conventional soft lithographic process (23).

To demonstrate the utility of CECE, we first designed a master containing an array of closed-loop structures. After the fabrication using two-photon absorption (TPA), PDMS is cast into the master (*SI Appendix*, Fig. S3*A*) to create a soft mold. PDMS was chosen because its curing dynamics can be easily controlled by adjusting the curing temperature and time (Fig. 1*B* and *SI Appendix*, Fig. S2). The polymerization and curing are carefully controlled to induce the crack formation at locked regions in the soft mold during peeling from the closed-loop master (see *SI Appendix*, section 1 for more details). As demonstrated in the SEM images (Fig. 1*C*), the prepared PDMS in phase I bears a large deformation and can be completely released from the closed-loop structure. In contrast, as shown in *SI Appendix*, Fig. S4*A*, without the introduction of phase I, the cracking was randomly formed in PDMS and both master and PDMS mold were damaged during the casting process. Moreover, the crack formed in phase I can be spontaneously opened (Fig. 1*D*) in phase II, making it possible to create many replicas based on one mold. On the other hand, without the introduction of phase II the crack formed in phase I is not stiff enough to self-seal; as shown in *SI Appendix*, Fig. S4*B*, thin membranes are observed in the replica and thereby blocking the hole of the loop during molding. Taken together, these experiments suggest that the principle of CECE is essential for the successful creation of hierarchical structures.

Mechanism Study. The controlled formation of crack for successful CECE should meet two criteria: 1) the crack should be preferentially formed in the PDMS mold rather than in the master. Moreover, the crack should develop along the direction of vertical peeling force; 2) the PDMS mold should be able to elastically deform and can be released completely from the closed-loop master. To provide a fundamental guidance for successful 3D replication, we then investigated the reproducible formation and configuration of the cracks in both phases I and II of CECE. In phase I, the geometry of the master determines the stress distribution in the PDMS, and thereby the eventual location and direction of cracking. To study how the geometric features of masters affect the crack formation, we developed a simple analytical model. As shown in Fig. 2*A*, we define a cracking coefficient $\eta = W_{min}/h$ to predict the location of the cracking, where W_{min} is the smallest width of the neck region and h is the height of the locked part. Similarly, to quantify the required maximum deformation of PDMS elastomer for its complete release from the master, we denote a deformation coefficient $\varphi = W_{min}/W_{max}$, where W_{max} is the largest width near the locked region. To provide guidance for the rational design of proper master structures, a phase diagram showing the effect of geometric parameters on the crack formation behavior is mapped out (Fig. 2*B*). The CECE will fail under the following two conditions: 1) when $\eta < 100\%$, the neck region breaks before the desired cracking emerges along the direction of peeling force; 2) when $1/\varphi < \varepsilon$ (where ε is the ultimate

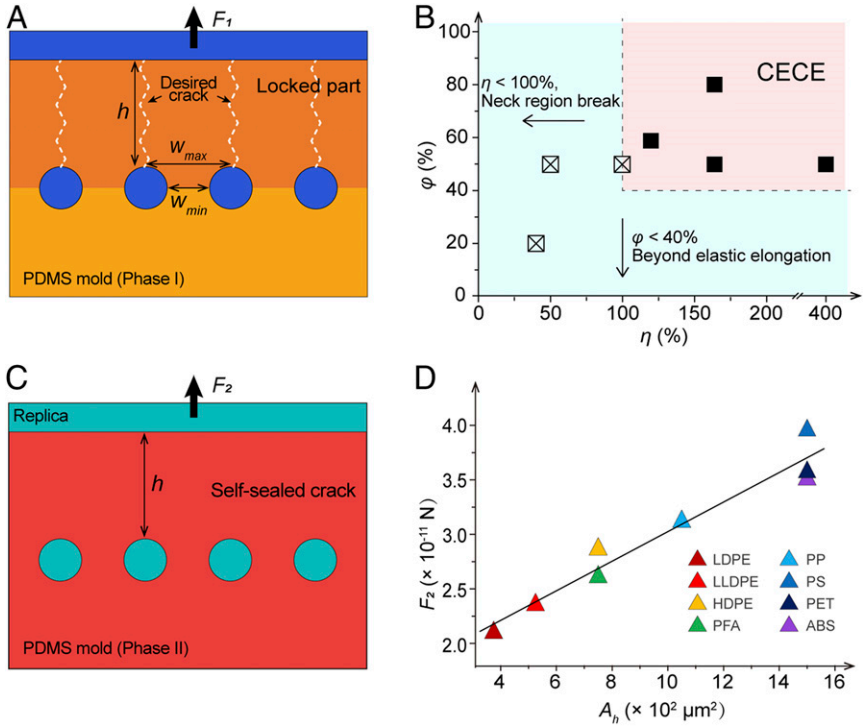

Fig. 2. Mechanism study. (*A* and *B*) Study of the controlled formation of elastic cracks in phase I. (*A*) A 2D model is simplified from the cross-sectional view of the closed-loop array for studying the crack formation process. Controlled crack formation takes place along the direction of the peeling force F_1; failure occurs when crack forms along the interface (referred to as neck region) of the locked part (darker orange). (*B*) A diagram predicting the controlled crack formation. The experimental and simulation results for the geometries are provided in *SI Appendix*, Fig. S6. (*C* and *D*) Study of configurable seal/open of the elastic cracks in phase II. (*C*) A geometric illustration showing the test of the configurability. The product loop is pulled out from the self-sealed elastic crack, and the yield point of the loop is checked. (*D*) The relationship between the critical force F_2 to open the cracks and the interfacial area A_h of the crack. The full names for the abbreviations of polymers are provided in *Materials and Methods*.

elongation of elastomer at break, ε = 250% for PDMS), the deformation of PDMS goes beyond its limit and as a result the mold cannot be released during the separation process. To validate our model, a series of PDMS molds were fabricated based on closed-loop masters with various geometries η and φ. Notably, the cracking behaviors observed in our experiments are consistent with the prediction shown in the phase diagram (*SI Appendix*, Figs. S5 and S6*A* and Table S1). We also performed finite-element analysis to further reveal the stress distribution in PDMS molds (*SI Appendix*, Fig. S6*B*). Indeed, an increase in either η or φ leads to both stronger stress and higher local deformation near the neck layer; otherwise, the stress distribution and the deformation shift to the bottom layer.

Based on a simple 2D model, we continued to evaluate the configurability of a sealed crack with a given interfacial area (A_h) by characterizing the required critical force (F_2) to open it (Fig. 2*C*). A 3D geometric illustration is also provided in *SI Appendix*, Fig. S7*A*. Briefly, we created a soft mold from a master containing a set of closed-loop structures with fixed height h = 15 μm, and different lengths l. Thus, the interfacial area of the crack can be expressed as $A_h = hl$. We used the mold to create replicas made of materials with various flexural strengths (σ). It is imaginable that in the demolding process the replica material has to be stiff enough to endure the drag during releasing through a crack in the mold. The replica loop structure with low σ and large l were observed to be misshaped because of this drag. Thus, we measured the maximum length of the faithful replicas and recorded it as the yield point of the material with specific σ (*SI Appendix*, Fig. S7*B*). At the yield point, the critical force can be expressed as $F_2 = \pi\sigma r^3/l$, where σ is the flexural strength of the replica material, and r is the radius of the closed loops (r = 2.5 μm). The critical force F_2 is found to be proportional to A_h, (that is, $\pi\sigma r^3/l \propto hl$) as plotted in Fig. 2*D*, indicating a good configurability of the sealing/opening of the elastic crack. Thus, for a given elastic crack, the required minimum flexural strength of the replica material can be calculated through $\sigma \propto hl^2/\pi r^3$ for guiding the material option. Our simulation suggests that the local stress in the PDMS mold is also smaller than the failure strength of PDMS during molding (*SI Appendix*, Fig. S8), making the reversible sealing and opening possible without damaging either the mold or the replicas.

To thoroughly evaluate the performance and merits of CECE, we further replicated a variety of representative 3D hierarchical structures (i.e., a beaded probe, a helix, an arch, a multibeam, a split ring, and a bull), resembling those emerging architectures with promising functions. The masters of these structures (*SI Appendix*, Fig. S3 *B–G*) were fabricated using prototyping methods that are expensive, time-consuming, and low throughput. More importantly, these 3D hierarchical structures have been proven challenging for replication using existing methods, owing to the presence of multiple pronged nanoscale shapes (i.e., closed loop, reentrant, high-aspect-ratio rods, and 3D arrays). For the doubly beaded probe shown in Fig. 3*A*, the aspect ratio (height/width) was measured to be 20, which is larger than those in most existing reports (25). We also successfully replicated a more complicated 2-cycle helix structure with high aspect ratio (Fig. 3*B*). This result nicely demonstrated the remarkable configurability of CECE via elastic deformation. To assess the lifespan of the elastic crack, we used 1 PDMS mold to repeatedly replicate an arch structure for cycles (Fig. 3*C*). Notably, the structure obtained after 50 cycles is still exactly identical with the master (*SI Appendix*, Fig. S9), demonstrating the superior robustness of our approach. As shown in Fig. 3 *D* and *E*, with CECE we were able to create structures with nanoscale beams and gaps, even down to 280 and 80 nm, respectively. Finally, a microbull, representing the most complicated arbitrary 3D structures producible using state-of-art techniques (12), can also be faithfully replicated (Fig. 3*F*), revealing the unprecedented capability of CECE and its full compatibility to initial prototyping techniques. *SI Appendix*, Table S2 summarizes a detailed comparison of characteristics between CECE and other fabrication methods. Taken together, it is clear that CECE is a unique technique for efficient and scalable replication of any 3D microstructures.

CECE for Construction of True 3D Hierarchical Biomimetic Materials. With the aid of CECE, we are able to construct virtually any 3D hierarchical structures to impart preferred functions. We first reproduced an artificial superomniphobic surface mimicking the soft, semitransparent, and liquid-repellent springtail skin (Fig. 4*A*). Fig. 4*B* shows the optical image of the as-fabricated, flexible, transparent polypropylene (PP) surface exhibiting excellent repellency to liquids even including hexane (surface tension: ~18.6 mN/m). In particular, the surface also displays a superior dynamic wetting property as evidenced by the complete rebounding of hexane droplet (Fig. 4*C*). Such a superior wetting property is ascribed to the presence of pillar arrays decorated with doubly reentrant structures (Fig. 4 *D* and *F*), which are faithfully transferred from their masters using CECE with the time and cost several orders of magnitude lower than those of standard 3D prototyping methods. Remarkably, owing to their strong flexibility and elastic deformation, these doubly reentrant structures preserve their

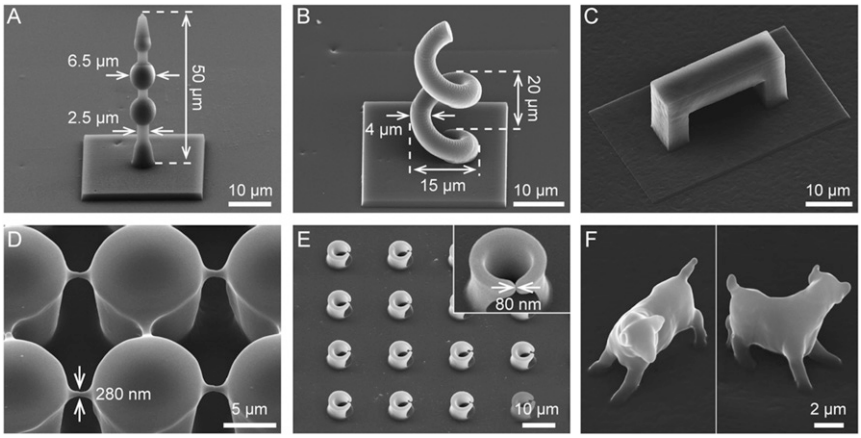

Fig. 3. True-3D hierarchical structures replicated by CECE. (*A*) A doubly beaded probe. (*B*) A helix with two cycles. (*C*) An arch. (*D*) An array of fine closed loops. (*E*) An array of split rings. (*F*) A microbull at two angles of view; such a structure represents the finest features achieved by 3D printing (12). The master structures for these replicas are shown in *SI Appendix*, Fig. S3. The methods for fabricating the master structures are described in *SI Appendix*, section 2.

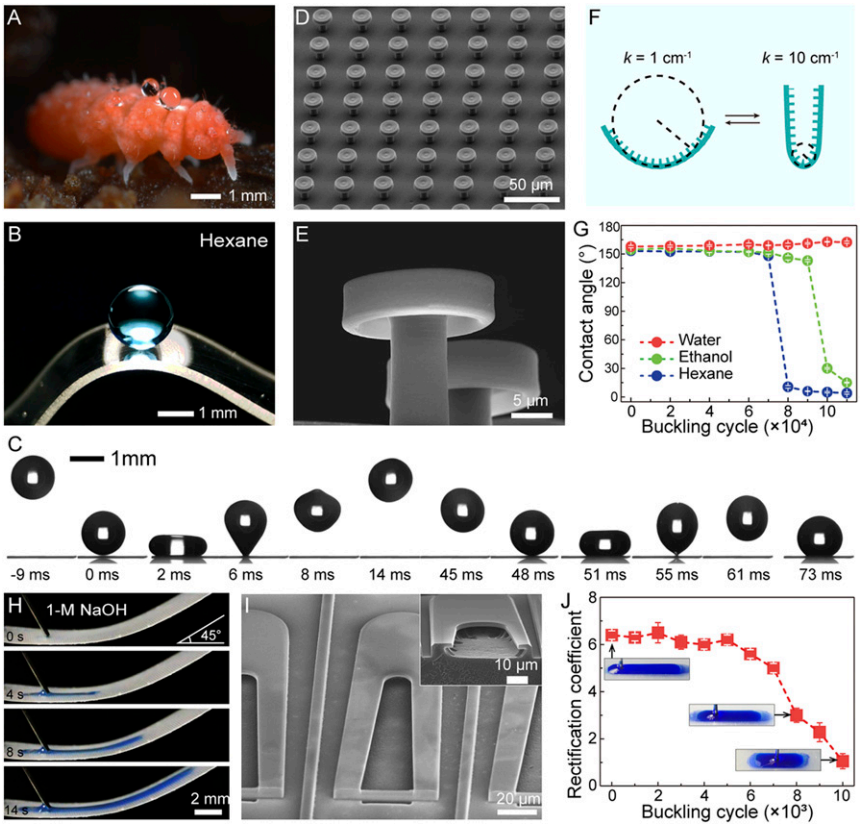

Fig. 4. Biomimetic materials construction. (*A–G*) A flexible and superomniphobic surface with doubly reentrant arrays mimicking the skin of springtail. (*A*) Optical image of a springtail with water droplets sitting on its skin. Image courtesy of Jan J. van Duinen (photographer). (*B*) Optical image of a blue-dyed hexane droplet sitting on the transparent and superomniphobic surface. (*C*) Time-lapse photographs showing a hexane droplet bouncing on the superomniphobic surface. (*D*) SEM image of the superomniphobic surface with an array of doubly reentrant structures. (*E*) Zoom-in image of the doubly reentrant structure. (*F*) Geometric illustration of the buckling model for the robustness test, where k is the curvature of the bent surface. (*G*) Evolution of contact angles of water, ethanol, and hexane on the superomniphobic along with the buckling cycles. (*H–J*) A flexible and anticorrosion liquid rectifier. (*H*) Time-lapse photographs showing 1 M NaOH solution directionally spreading upward on a curved rectifier. The solution was fed onto the surface at a rate of 20 μL/min. (*I*) SEM image of the as-fabricated plastic rectifier. (*Inset*) A cross-sectional view of the reentrant structure. (*J*) Evolution of the rectification coefficient of the liquid rectifier during the robustness test against buckling.

structural integrity and liquid repellence during repeated bending deformation. The bending test was conducted by using a buckling device (Movie S1) with defined curvatures (k, as illustrated in Fig. 4*F*) at a frequency of 50 cycles per minute. For water and ultralow-surface-tension liquids (e.g., ethanol and hexane), we did not observe obvious decay in the dynamic wetting property until the buckling cycles are up to 100,000 and 70,000, respectively (Fig. 4*G* and Movie S1). In contrast, for the counterparts based on rigid materials, the surfaces are easily broken, and their liquid repellences are lost after only several cycles of buckling. These complicated reentrant structures can also be fabricated on other chemically inert materials, e.g., polyethylene (PE), thus offering the potential to achieve a wide range of functionalities.

Fig. 4*H* and Movie S2 show the spontaneous and directional spreading of 1 M NaOH liquid along the as-fabricated liquid-diode device based on PE material. Different from the liquid diode fabricated on rigid silicon, the use of PE substrate not only endows a high degree of flexibility, but also imparts enhanced chemical stability against corrosives. Fig. 4*I* shows the morphology of the PE rectifier, which is orderly decorated with capillary channels and reentrant structures (highlighted by Fig. 4 *I*, *Inset*). The liquid diode displays very stable liquid rectification performance even after 6,000 buckling cycles, suggesting its unprecedented robustness (Fig. 4*J*). Such a flexible and mechanochemically robust rectifier is potentially suitable for adhering onto complex surfaces—in the form of adhesive tape—for the directional transport of diverse fluids.

Conclusions

Taken together, we have demonstrated that CECE imparts various important merits—including broad material compatibility, high resolution, rapid and mass production, high accessibility, and low cost—for the construction of true 3D architectures. In particular, CECE expands the capability of material choices from limited base materials (e.g., Si and photoresist) to a broad range of engineering materials [e.g., polymers, and other printable materials including SiO_2 (26), metal (27), ceramic (28)]. Therefore, CECE promises to pave the road for transferring biomimetic materials into real-world applications. We expect further breakthrough with CECE in several directions. For example, we can further extend the complexity of processible structures [e.g., an array of microhelixes (29)] by using more broadly tunable mold materials or realize greater diversity of functions (e.g., self-adaptive, layer-heterogenic, stimuli-responsive, time-programmed) by creating structures of hybrid or composite materials (30). In a wider scope, we anticipate that further fundamental study on the configurability of elastic cracks in terms of their orientation, length, and width would help advance the nanotechnologies (20–22) for precise and scalable pattern formation in a broad range from atomic to macroscale.

Materials and Methods

Elastic Crack Formation. The elastic crack was generated by using modified soft lithography by controlling the curing dynamics of PDMS. First, RTV 615 PDMS (General Electric) was thoroughly mixed in a 10:1 mass ratio of

prepolymer to curing agent and degassed in a vacuum desiccator for 30 min. Then, the PDMS mixture was poured on the closed-loop master and cured at room temperature (22 °C) for 24 h (denoted as phase I). Note that PDMS would cure sufficiently in 24 h at 25 °C to permit handling, while the time window for the operation could be extended to 48 h. After that, the elastic crack was formed by carefully peeling off the cured PDMS. The PDMS was then baked for 30 min at 150 °C (denoted as phase II). The temperature was gradually raised (typically 10 °C per minute) from room temperature at the beginning of baking.

CECE-Assisted Molding Process. The configurability of the elastic crack was utilized for replication of true 3D hierarchical structures. The casting step was conducted according to the procedure for the crack formation. Then the PDMS mold was attached on a glass slide for molding thermoplastic plate. The thermoplastic plate was hot-pressed with the PDMS mold at molten state for 1 min under a pressure of ∼0.2 MPa. After that, the sandwich was cooled down to room temperature gradually while the pressure was kept. The product replica was obtained after the PDMS mold was peeled off. Thermoplastic materials such as low-density polyethylene (LDPE), linear low-density polyethylene (LLDPE), high-density polyethylene, PP, PS, fluorinated ethylene propylene (FEP), polyethylene terephthalate (PET), and acrylonitrile butadiene styrene copolymers were employed for molding a set of beam structures with lengths.

Biomimetic Materials Construction. The doubly reentrant structure was fabricated by TPA and then transfer-printed to PP material. The fabrication details are illustrated in *SI Appendix*, Fig. S10. The liquid repellency was evaluated by testing the rebound of water, ethanol, and hexane droplets under Weber number ∼0.5. The contact angles of the droplets were measured when the liquids reached static. The silicon liquid rectifier was fabricated using standard MEMS process, as described elsewhere (3), and then transfer-printed to PE material. The PE liquid rectifier was then treated with air plasma to decrease the apparent contact angles of water to ∼15°. Then, 1 M NaOH aqueous solution was fed onto the surface of the rectifier at a velocity of 20 μL/min, and the spreading behavior was recorded with a camera.

Mechanical Robustness Test. The robustness of the biomimetic materials was tested using a homemade buckling device. A strip (20 mm × 5 mm × 0.1 mm) was fixed on the device and was buckled repeatedly at a frequency of 50 times per minute. The curvature of the tested strip was repeatedly changed between 10 cm^{-1} and 1 cm^{-1}. The liquid contact angles and the rectification coefficient were measured after every 1,000 buckling cycles for monitoring the liquid repellency of the superomniphobic material and the transport performance of the liquid rectifier, respectively.

Data Availability. All materials, methods, and data needed to evaluate the conclusions are present in the main article and/or *SI Appendix*.

ACKNOWLEDGMENTS. This work was supported by National Natural Science Foundation of China (51773173), Hong Kong Baptist University (FRG2/17-18/102, SDF 03-17-096, RC-IRMS/16-17/03), Hong Kong Research Grants Council (C1018-17G, 22200515, 11218417), and the Hong Kong Baptist University (HKBU), State Key Laboratory of Environmental and Biological Analysis, "State Key Laboratory - Collaborative Research Fund" (SKLP_1718_P01). We acknowledge Surface Analysis & Material Characterization Laboratory of HKBU for the SEM characterization and Nanosystem Fabrication Facility (NFF) of Hong Kong University of Science and Technology for the 3D laser lithography fabrication.

1. R. Hensel *et al*., Wetting resistance at its topographical limit: The benefit of mushroom and serif T structures. *Langmuir* **29**, 1100–1112 (2013).
2. G. T. Yun *et al*., Springtail-inspired superomniphobic surface with extreme pressure resistance. *Sci. Adv.* **4**, eaat4978 (2018).
3. J. Li *et al*., Topological liquid diode. *Sci. Adv.* **3**, eaao3530 (2017).
4. J. Li *et al*., Designing biomimetic liquid diodes. *Soft Matter* **15**, 1902–1915 (2019).
5. R. Helbig, J. Nickerl, C. Neinhuis, C. Werner, Smart skin patterns protect springtails. *PLoS One* **6**, e25105 (2011).
6. H. F. Bohn, W. Federle, Insect aquaplaning: Nepenthes pitcher plants capture prey with the peristome, a fully wettable water-lubricated anisotropic surface. *Proc. Natl. Acad. Sci. U.S.A.* **101**, 14138–14143 (2004).
7. H. Chen *et al*., Continuous directional water transport on the peristome surface of Nepenthes alata. *Nature* **532**, 85–89 (2016).
8. K. Autumn *et al*., Adhesive force of a single gecko foot-hair. *Nature* **405**, 681–685 (2000).
9. A. K. Geim *et al*., Microfabricated adhesive mimicking gecko foot-hair. *Nat. Mater.* **2**, 461–463 (2003).
10. E. Arzt, S. Gorb, R. Spolenak, From micro to nano contacts in biological attachment devices. *Proc. Natl. Acad. Sci. U.S.A.* **100**, 10603–10606 (2003).
11. H. Gao, H. Yao, Shape insensitive optimal adhesion of nanoscale fibrillar structures. *Proc. Natl. Acad. Sci. U.S.A.* **101**, 7851–7856 (2004).
12. S. Kawata, H.-B. Sun, T. Tanaka, K. Takada, Finer features for functional microdevices. *Nature* **412**, 697–698 (2001).
13. P. Vukusic, J. R. Sambles, Photonic structures in biology. *Nature* **424**, 852–855 (2003).
14. J. Aizenberg, A. Tkachenko, S. Weiner, L. Addadi, G. Hendler, Calcitic microlenses as part of the photoreceptor system in brittlestars. *Nature* **412**, 819–822 (2001).
15. M. Eder, S. Amini, P. Fratzl, Biological composites-complex structures for functional diversity. *Science* **362**, 543–547 (2018).
16. A. Tuteja *et al*., Designing superoleophobic surfaces. *Science* **318**, 1618–1622 (2007).
17. T. L. Liu, C. J. Kim, Repellent surfaces. Turning a surface superrepellent even to completely wetting liquids. *Science* **346**, 1096–1100 (2014).
18. J. Shim *et al*., Controlled crack propagation for atomic precision handling of wafer-scale two-dimensional materials. *Science* **362**, 665–670 (2018).
19. H. Kim *et al*., Flexible elastomer patch with vertical silicon nanoneedles for intracellular and intratissue nanoinjection of biomolecules. *Sci. Adv.* **4**, eaau6972 (2018).
20. D. Kang *et al*., Ultrasensitive mechanical crack-based sensor inspired by the spider sensory system. *Nature* **516**, 222–226 (2014).
21. K. H. Nam, I. H. Park, S. H. Ko, Patterning by controlled cracking. *Nature* **485**, 221–224 (2012).
22. X. Zhu *et al*., Fabrication of reconfigurable protein matrices by cracking. *Nat. Mater.* **4**, 403–406 (2005).
23. D. Qin, Y. Xia, G. M. Whitesides, Soft lithography for micro- and nanoscale patterning. *Nat. Protoc.* **5**, 491–502 (2010).
24. E. J. Wong, "Modeling and control of rapid cure in polydimethylsiloxane (PDMS) for microfluidic device applications" PhD dissertation, Massachusetts Institute of Technology, Cambridge, MA (2010).
25. D. Rajput, L. Costa, K. Lansford, A. Terekhov, W. Hofmeister, Solution-cast high-aspect-ratio polymer structures from direct-write templates. *ACS Appl. Mater. Interfaces* **5**, 1–5 (2013).
26. F. Kotz *et al*., Three-dimensional printing of transparent fused silica glass. *Nature* **544**, 337–339 (2017).
27. C. Ladd, J. H. So, J. Muth, M. D. Dickey, 3D printing of free standing liquid metal microstructures. *Adv. Mater.* **25**, 5081–5085 (2013).
28. G. Liu, Y. Zhao, G. Wu, J. Lu, Origami and 4D printing of elastomer-derived ceramic structures. *Sci. Adv.* **4**, eaat0641 (2018).
29. J. K. Gansel *et al*., Gold helix photonic metamaterial as broadband circular polarizer. *Science* **325**, 1513–1515 (2009).
30. A. G. Mark, J. G. Gibbs, T. C. Lee, P. Fischer, Hybrid nanocolloids with programmed three-dimensional shape and material composition. *Nat. Mater.* **12**, 802–807 (2013).